Powder Technology 366 (2020) 859–872

Contents lists available at ScienceDirect

Powder Technology

journal homepage: www.elsevier.com/locate/powtec

Design and proof of concept of a continuous pressurized multi-stage fluidized bed setup for deep sour gas removal using adsorption

Rick T. Driessen *, Benno Knaken, Tim Buzink, Daan A.F. Jacobs, Juraj Hrstka, Derk W.F. Brilman *

Sustainable Process Technology, Faculty of Science and Technology, University of Twente, PO Box 217, 7500 AE Enschede, the Netherlands

ARTICLE INFO

Article history:
Received 12 July 2019
Received in revised form 11 December 2019
Accepted 4 March 2020
Available online 6 March 2020

Keywords:
Multi-stage fluidized bed
Pressure swing adsorption
Amine sorbent
Particle model
Natural gas
Lewatit VP OC 1065

ABSTRACT

Pressure swing adsorption (PSA) processes are frequently used in the (petro)chemical industry, but they suffer from ineffective use of the sorbent and slow heat transfer. A pressurized multi-stage fluidized bed (MSFB) for continuous PSA is proposed in this work to overcome these drawbacks. A one stage fluidized bed adsorber was used to determine minimum fluidization velocities of the used amine sorbent at various pressures up to 10 bara. The design of a pilot scale experimental setup is described, together with supporting experiments to show the proof of concept. Removal from 37,000 mol ppm CO_2 to <10 mol ppm CO_2 in a few seconds was demonstrated in the pressurized MSFB adsorber. The tray efficiencies were high: often larger than 0.85. Using a numerical particle model, it was concluded that the CO_2 adsorption rate is controlled via intraparticle mass transfer.

1. Introduction

Adsorption is a widely used separation technology in the (petro) chemical industry. The conventional setup for an adsorption process are multiple fixed beds interconnected in a certain sequence to enable adsorption and desorption. The desorption can be effected by elevating the temperature, temperature swing adsorption (TSA), or by lowering the pressure, pressure swing adsorption (PSA). Although that fixed bed adsorption is an industrially established process, it has some disadvantages:

1. Ineffective use of sorbent: In a fixed bed adsorption process only the sorbent in the mass transfer zone is active [1]. The sorbent upstream of the mass transfer zone is already at its equilibrium loading and the sorbent downstream of the mass transfer zone does not see any adsorbates. As a consequence, the effective use of the sorbent is quite low, which results in large equipment.
2. Slow heat transfer: When using TSA, heat has to be supplied to the fixed bed while fixed beds generally show slow heat transfer. This implies that heating the fixed bed to the desired temperature takes a considerable amount of time or measures have to be taken to enhance heat transfer, for example by using a multi-tubular fixed bed.

To overcome the ineffective use of the sorbent, one can think of continuous adsorption processes where the solid sorbent circulates between an adsorption and desorption zone. In this way the amount of sorbent which is in an inactive zone is minimized. Continuous adsorption processes exist for a while. Kunii and Levenspiel name some examples where carbon is used to clean a variety of gases with low adsorbate concentrations (<0.1%) [2]. Recently, continuous adsorption processes received renewed attention in view of post-combustion carbon dioxide (CO_2) capture. Veneman et al. use a gas-solid trickle flow reactor to adsorb CO_2 and use a multi-stage fluidized bed for desorption [3]. Multiple researchers investigated the use of multi-stage fluidized beds for post-combustion CO_2 capture. For a full review of these papers we refer to our earlier work [4], but we want to highlight some. The group of Meikap investigate multi-stage fluidized beds experimentally with various sorbents [5,6]. The group of Hofbauer and Schöny built a bench scale multi-stage fluidized bed and present their first experimental results [7–9].

All these researchers use continuous processes with TSA to adsorb CO_2 from gaseous streams. However, the use of PSA in a continuous sorbent process has not yet been investigated to our knowledge. This work focuses on the adsorption of sour gases from pressurized gases ($P > 1$ atm) in a system where the sorbent circulates. This is schematically shown in Fig. 1. The adsorber is operated at elevated pressure, in this work typically at 10 bara, whereas the desorber is operated at lower pressure, in this work typically at 1 bara. The challenge in this continuous experimental setup is to pressurize the sorbent before it enters the adsorber and to depressurize the sorbent after it leaves the adsorber.

* Corresponding authors.
E-mail addresses: r.t.driessen@utwente.nl (R.T. Driessen), wim.brilman@utwente.nl (D.W.F. Brilman).

https://doi.org/10.1016/j.powtec.2020.03.013
0032-5910/

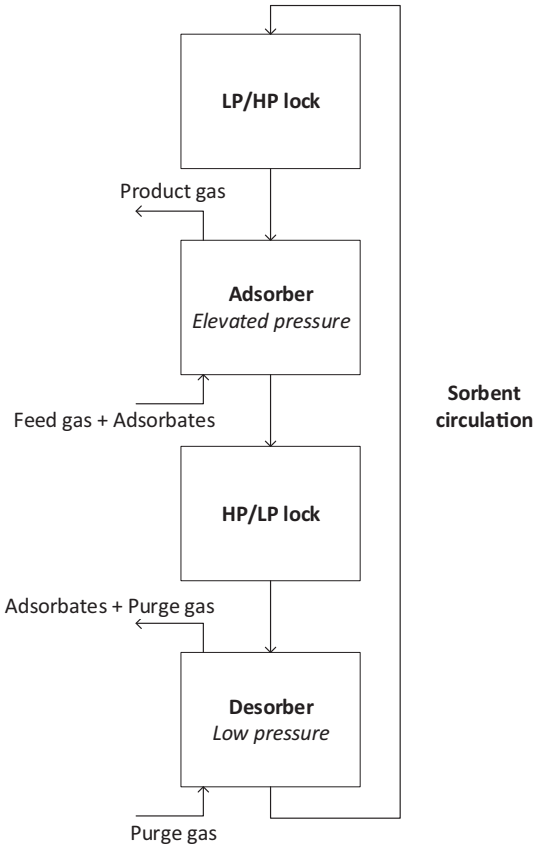

Fig. 1. Conceptual scheme of a continuous adsorption process employing a pressure swing. The adsorber is operated at elevated pressure, whereas the desorber operates at a lower pressure. The sorbent has to be pressurized and depressurized which is facilitated by the low pressure/high pressure (LP/HP) lock and high pressure/low pressure (HP/LP) lock respectively.

This is facilitated by a so-called low pressure/high pressure (LP/HP) lock and a high pressure/low pressure (HP/LP) lock respectively. Without further detailed technical explanations, these locks are unit operations in which solid particles are pressurized or depressurized.

In this work a continuous process is investigated in the context of sour gas removal (hydrogen sulfide and carbon dioxide) from natural gas. At the moment the benchmark process for sour gas removal from natural gas is scrubbing employing aqueous amines, such as methyldiethanolamine (MDEA). The proposed adsorption process could reduce equipment size because mass transfer in the gas phase is generally faster than mass transfer in the liquid phase. Also, it could reduce the energy consumption because solid adsorbents have a lower specific heat capacity than aqueous solutions. In short, using the proposed adsorption instead of absorption can reduce the capital and operational expenditure of the sour gas removal process [4].

In the context of sour gas removal from natural gas, we would like to present three arguments why PSA is required. First, the adsorption equilibrium is favored by higher pressures. Therefore, it is advantageous to adsorb the sour gas at elevated pressures similar to the gas well pressure. Second, the specifications for product natural gas (so called 'sweet gas') are tight: hydrogen sulfide (H_2S) has to be removed down to 3.5 ppm and CO_2 typically down to 1%. For liquefied natural gas applications the CO_2 specification is even lower: 50 ppm [10]. These low sour gas specifications require that the lean sorbent loading, the amount of sour gas adsorbed on the regenerated sorbent, is also very low: otherwise the gas specifications in the adsorber outlet cannot be reached. Third, from an industrial perspective, it may be desirable to use steam as stripping gas in the desorber: steam can be condensed to obtain a concentrated stream of H_2S and CO_2. However, if the desorption is performed with steam at a pressure equal to the gas well (for example, 60 bara), the temperature in the desorber would be larger than 270 °C to ensure that water remains in the vapour phase. This temperature is above the thermal stability limit of amine sorbents, which is typically around 150 °C [11]. Therefore, it is necessary to lower the absolute pressure in the desorber. In short, lowering the absolute pressure in the desorber is required.

This works introduces the concept of a pressurized multi-stage fluidized bed adsorber working together with a atmospheric multi-stage fluidized bed desorber. To our knowledge, this principle has never been demonstrated or researched in open literature. A bench-scale one stage fluidized bed without sorbent circulation was used to obtain basic design data such as minimum fluidization velocities. Furthermore, adsorption breakthrough curves were measured to test the feasibility of the technology in an early stage. The design of the continuous pressurized multi-stage fluidized bed experimental setup will be elaborated on. A series of measurements was conducted in the continuous pressurized MSFB which confirms the technical proof-of-concept. A numerical particle model was used to interpret the experimental data to investigate the various mass transfer processes inside and outside of the particle.

2. One stage fluidized bed adsorber

2.1. Materials

The amine sorbent used in this work is Lewatit VP OC 1065 (Lanxess). The polystyrene backbone of this sorbent is cross-linked with 8%–10% divinylbenzene and functionalized with benzylamine sidegroups. These sidegroups provide the function to adsorb H_2S and CO_2. The amine sorbent was mixed with graphite powder (0.3 wt%) to eliminate electrostatic forces. With respect to fluidization behaviour, Lewatit VP OC 1065 is classified as a Geldart B particle [4]. In this work the CO_2 adsorption isotherm of Bos et al. is used to evaluate the CO_2 sorbent loading at equilibrium [12]. The particle size distribution (PSD) of the amine sorbent was measured using a dynamic light scattering technique with a Malvern Mastersizer 2000. More detailed information on physical properties can be found in earlier published work [3,4,13].

For safety reasons, methane (the main compound of natural gas) is not used. Instead, nitrogen (grade 4.7, purity >99.997 vol%) (N_2) is used to mimic methane. This is possible because neither methane nor nitrogen do adsorb on the amine sorbent [14,15]. CO_2 (grade 2.7, purity > 99.7 vol%) is used as sour gas compound.

2.2. Experimental setup

Fig. 2 shows a schematic of the one stage fluidized bed adsorber. The main component of this experimental setup is a gas-solid fluidized bed contactor (400 mm height, 50 mm inner diameter). This contactor is equipped with a metal sintered plate to ensure the gas distribution. Two sight glasses are installed for visual inspection of the fluidized bed. K-type thermocouples (TI-1 to TI-5) are installed in five thermowells at different axial positions. Two mass flow controllers (MFCs) control the gas flow: an Alicat MCR-500SLPM-D MFC for N_2 and an Alicat MCS-5SLPM-D for CO_2. A three-way valve (V1) provides the option to measure the inlet concentration over the bypass or to send the gas to the gas-solid contactor. The inlet and outlet pressure are measured via pressure transducers (PI-1 and PI-4). Pressures up to 10 bara could be set via a back pressure regulator (BPR). A LI-COR LI-840A CO_2 analyzer, calibrated in the range 0 — 10000 mol ppm, is used to measure the CO_2 concentration.

The minimum fluidization velocity is measured via a pressure drop measurement. A differential pressure transducer (BD| Sensors DMD 341, 0–20 mbar) measures the pressure drop over the fluidized bed, according to the connections of DP-1 in Fig. 2. Before determining the minimum fluidization velocity, the sorbent was desorbed according to the procedure described below. The minimum fluidization velocity was

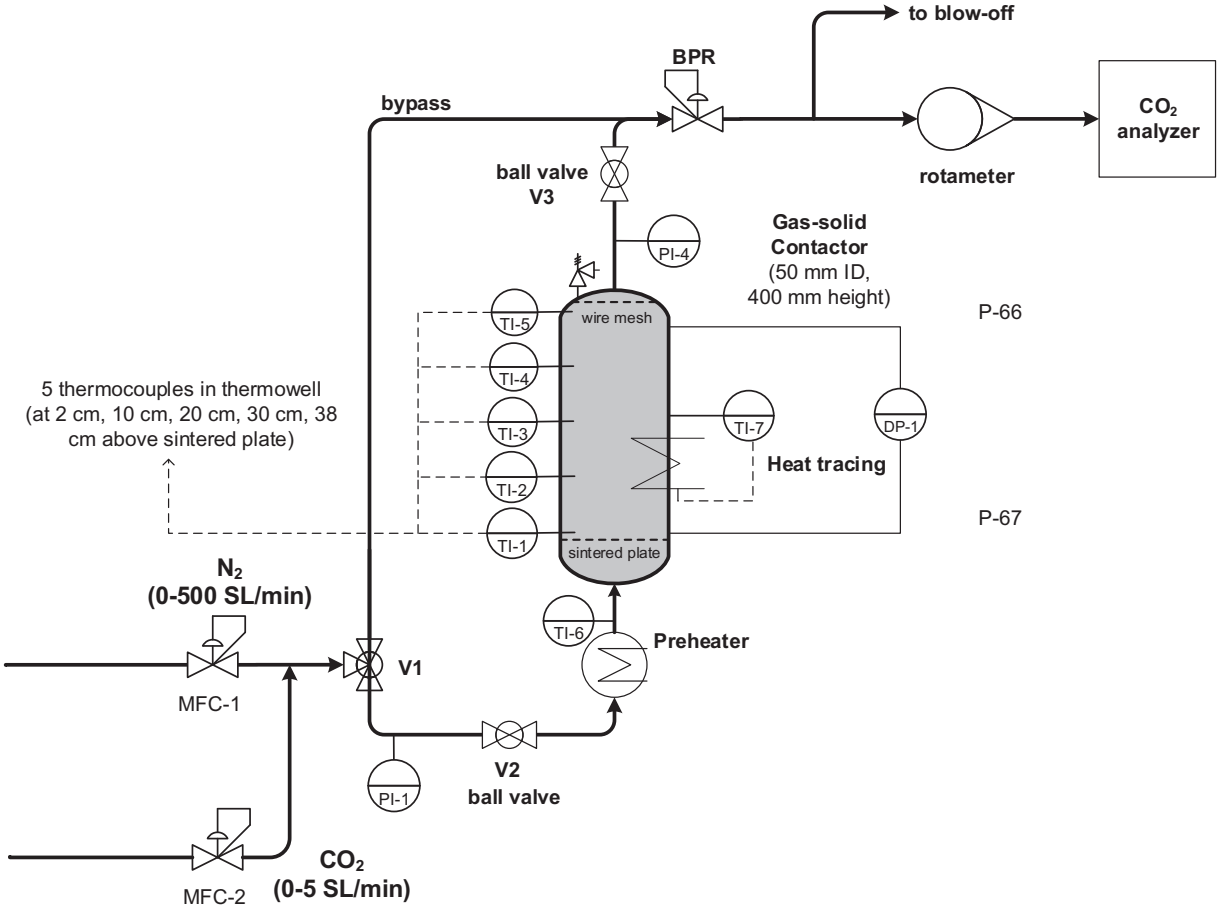

Fig. 2. Schematic of the one stage fluidized bed adsorber.

determined for various pressures, ranging from 2.5 to 10.0 bara. The fixed bed height was 0.226 m for every measurement. Hysteresis effects were checked by first increasing the superficial velocity and then by decreasing the superficial velocity while measuring the pressure drop. For each superficial velocity the pressure drop was averaged over a time period of at least 40 s.

A breakthrough adsorption experiment was always started via desorption to make sure that the sorbent loading is null. The column was depressurized step-wise from 10 bara to 2 bara while adjusting the N_2 flow to ensure proper fluidization and, thus, heat transfer. In the end, the desorption was said to be finished if the CO_2 concentration was less than 3 mol ppm for at least 120 s at a pressure of 2 bara. After this event the heaters were turned off, the column was pressurized to 10 bara with a N_2 flow of 80 SL/min, to cool the sorbent. Before starting the adsorption the column is pressurized with N_2. Once the column was pressurized, the bypass is used to set desired the inlet concentration and flows by configuring the setpoints of the MFCs. If the setpoints were obtained, the CO_2 flow was shut off and the column was fluidized with N_2. The start of the experiment is defined as the moment at which CO_2 is sent to the column. The dead time, defined as the time difference between CO_2 introduction and the first CO_2 signal on the CO_2 analyzer, was estimated. The sorbent in the column was mimicked with glass beads and a fictive adsorption measurement was started. The determined dead time was 8 s and was found to be independent of the superficial velocity. All presented results are corrected for the dead time. The fixed bed height of the sorbent was 0.226 m. The pressure is varied between 2.5 and 10.0 bara and the superficial velocity was kept constant at $u_0 = 1.5u_{mf}$.

2.3. Setup design

Based on the conceptual scheme in Fig. 1 an experimental setup was designed and built in the High Pressure Laboratory of the University of Twente. The setup is protected by a Plexiglas case which is maintained at underpressure relative to the surroundings, this means that this setup allows for future operation with hazardous gases including H_2S. A photo of the setup is shown in Fig. 3. The two left columns of the casing contain caustic scrubbers, which are meant for safeguarding for emissions of H_2S but are not used in this work. The right-hand and tallest column of the casing case contains the experimental setup. The dimensions of this case are $0.8 \times 0.8 \times 7.0$ m (L × W × H).

2.4. General layout of the pilot plant

Fig. 4 shows a process flow diagram (PFD) of the experimental setup. In reality, the PFD is more complex because it includes, among others, various thermocouples, safety valves and level indicators. These components are left out for the sake of simplicity. The key units of the experimental setup are: a LP/HP lock to pressurize the sorbent, the pressurized MSFB adsorber, a HP/LP lock to depressurize the sorbent, an atmospheric MSFB desorber and a riser. First, the operation of pilot plant is explained and thereafter some key units are explained in more detail.

Lean sorbent is transported in a riser (20 mm inner diameter) with N_2 as transport gas at a linear velocity of ~5 m/s. The riser flow is regulated and measured with a SMC PFM711S-F02-F flow switch. A cyclone separates the riser gas from the sorbent. The sorbent is collected in a buffer vessel. The LP/HP lock pressurizes the sorbent by sequential switching of valves, which is explained in more detail in *sec*:locks.

Fig. 3. Picture of the experimental pressurized MSFB setup: the right case contains the actual setup.

The pressurized sorbent is transported to another buffer vessel before it is dosed in the pressurized MSFB adsorber using a rotary valve. The adsorber is fed with a N_2/CO_2-mixture. The bottom of the adsorber functions as a buffer. The rich sorbent is transported from the adsorber to the HP/LP lock where it is depressurized. Again a buffer vessel is used before the amine sorbent is dosed in the desorber with a rotary valve. After desorption in the desorber the lean sorbent is transported back with the riser to the top of the pilot plant.

The control of the setup and data logging is automated with a custom-made program in NI LabVIEW 2017 SP1. All valves that required automatic switching are pneumatically controlled with a Metal Work Multimach electropneumatic distribution block. Mass flow controllers (Brooks Instrument, SLA-series) were used to control the gas flows in the adsorber. An Alicat MCR-500 mass flow controller was used to control the N_2-flow to the desorber. All rotary valves (Rotolok Rotary Airlock 50 mm) are driven by a alternating current electric motor.

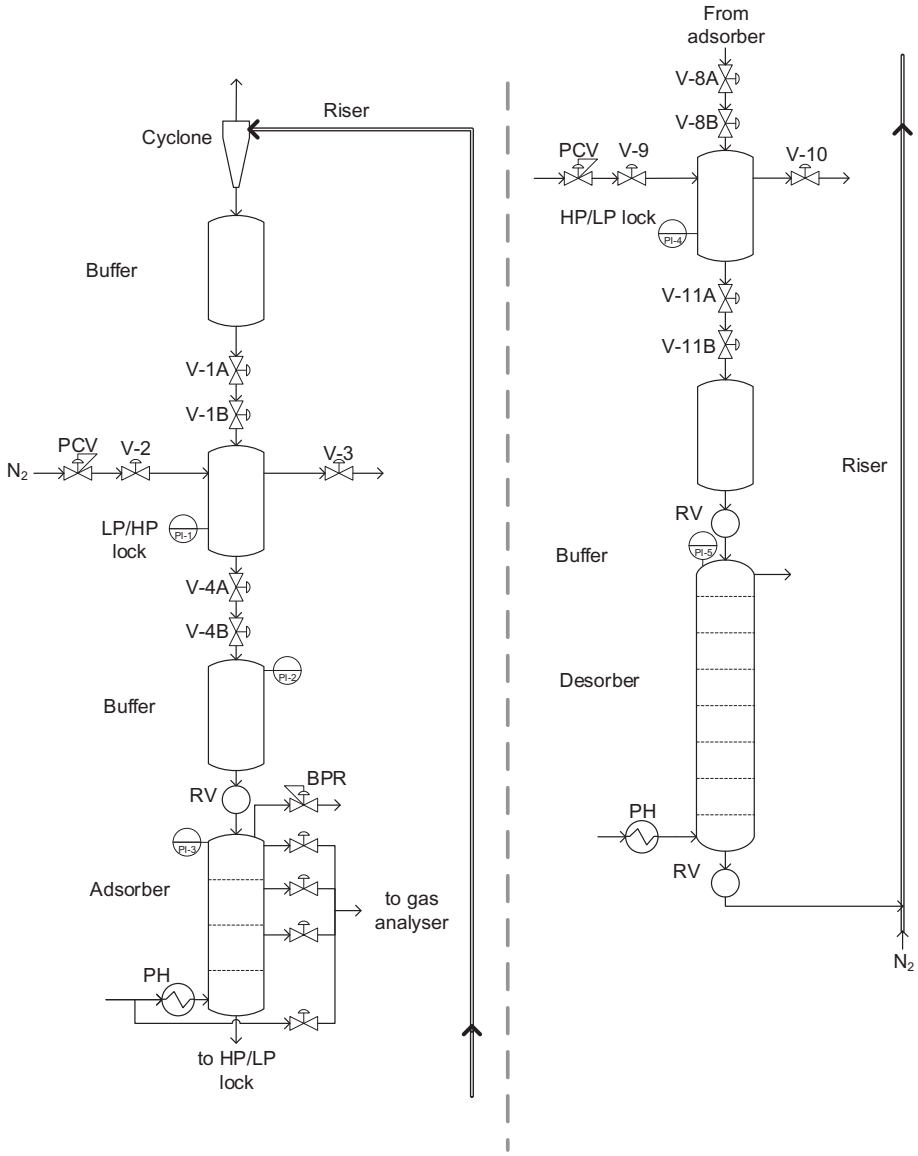

Fig. 4. Process flow diagram of the experimental setup. Please note that it is divided in the upper (left) and lower (right) part, but the actual arrangement is vertical. (BPR = back pressure regulator, PCV = pressure control valve, pH = preheater, PI = pressure indicator, RV = rotary valve, V = ball valve).

Dependent on the CO_2-concentrations, various CO_2-analyzers were used to analyze compositions: a Siemens ULTRAMAT 23 (0−250 ppm CO_2) gas analyzer, a LI-COR LI-840 (0−10, 000 ppm CO_2) CO_2-analyzer and a Sick Maihak Sidor S700 (0−15% CO_2). All analyzers were calibrated in the respective concentration ranges with calibration gases.

2.5. Low pressure/high pressure (LP/HP) and high pressure/low pressure (HP/LP) locks

Because an absolute pressure swing is applied the amine sorbent has to be pressurized and depressurized to enable sorbent circulation through different pressure levels. In this work we chose to pressurize the sorbent with N2 as inert gas. Both locks work sequentially; for the LP/HP lock the sequence is:

1. Ball valves V-1A and V-1B open to fill the vessel with amine sorbent.
2. Ball valve V-2 is opened and the vessel is pressurized with N_2. The pressure of N_2 is set with a pressure control valve (PCV). After the pressure setpoint of pressure indicator 1 (PI-1) has been reached, valve V-2 closes.
3. Ball valves V-4A and V-4B open and the pressurized amine sorbent is emptied in the buffer vessel below.
4. Ball valve V-3 opens to depressurize the vessel. It closes again if the lower pressure setpoint has been reached.
5. The sequence repeats beginning with the first step.

For depressurizing the sorbent, the HP/LP lock works in a similar sequence but reversely.

Before building the setup preliminary tests with ball valves with Teflon seats were performed to investigate if the seats of the ball valve would wear due to the sorbent particles. Via a pressure test it was readily find out that the seats do indeed wear: the gas seal of the ball valve could not be ensured. Therefore, we chose to use two ball valves in series for ball valves V-1A/B and V-4A/B. The first ball valve (V-1A and V-4A respectively) switch the sorbent flow, which means that the second ball valves (V-1B and V-4B respectively) can switch in a 'sorbent free' environment. This ensures that the seats of the second ball valves

do not wear. Ideally, one would like to install one valve that (a) starts and stops the sorbent flow and (b) ensures the gas seal. To our knowledge, such valves do not yet exist and, thus, we chose this option to show the working principle of a pressurized MSFB. Furthermore, ball valves are cheap in case replacement of the ball valves is required. So far, this was not needed in approximately 350 h of operating time.

The volume of both locks is approximately 2 L. The typical filling and emptying time was 10 s for all solid fluxes. The setpoint of the pressure control valves was 1 bar above the adsorber pressure. Stainless steel full bore ball valves of 0.5 in. with Teflon seats were used for ball valves V-1A/B, V-4A/B, V-8A/B and V-11A/B.

2.6. Pressurized multi-stage fluidized bed (MSFB) adsorber

The core unit of the pilot plant is the pressurized MSFB adsorber. A detailed schematic of the adsorber can be found in Fig. 5. The MSFB adsorber consists of three stages and has an inner diameter of 50 mm. The inner diameter is rather low because a certain superficial velocity has to be maintained to enable fluidization and the N_2-flow is limited in our available facilities. The pressure is regulated via a back pressure regulator (Dutch Regulators GBT15S-50 N20-SSEE). The distance between two perforated plates is 200 mm. The height of the downcomers (20 mm inner diameter) could be adjusted to also measure the effect of bed heights. Horizontal plates with a diameter equal to the outer diameter of the downcomer were installed 16 mm below the bottom of the downcomer. The latter is needed to prevent excessive fluidization in the downcomer.

The bottom tray ($n = 1$) is equipped with a metal sintered plate as gas distributor. The other trays ($n = 1$ and $n = 2$) have a perforated plate as gas distributor. For a specific measurement the pressure drop across stage $n = 2$ (that is, the perforated plate and the fluidized bed) was measured using a differential pressure transducer (BD| Sensors DMD 341, 0–20 mbar) by connecting it two the sample points at stage $n = 1$ and $n = 2$. Each tray is equipped with sampling points to analyze the composition at that tray. Thermowells with K-type thermocouples are installed at each stage 20 mm above the gas distributor to measure the bed temperature. Sight glasses allow for visual observation of the tray. The adsorber wall was encircled with a tube connected to a cooling bath (Julabo F25-MW) filled with water to allow for cooling. The setpoint of the cooling bath was 10, but it was readily observed that the cooling bath did not have enough power to cool it to the setpoint. Typically, the water temperature of the cooling bath was 18–20 °C.

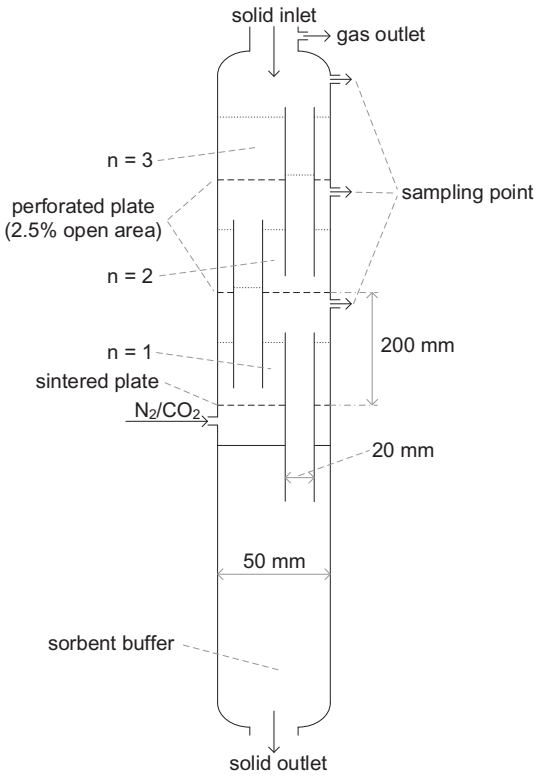

Fig. 5. Schematic of the internals of the MSFB adsorber with the most important dimensions. The configuration of the bottom of the downcomers is shown in Fig. 6. The dotted lines denote the top level of the fluidized bed. The stage number is denoted by *n*.

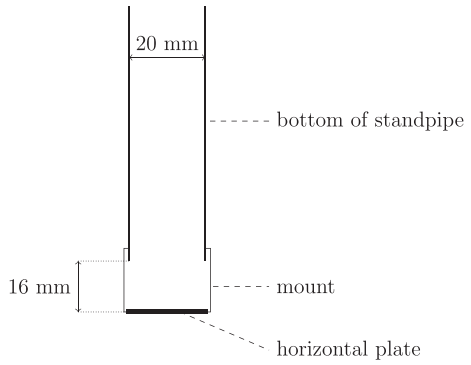

Fig. 6. The configuration of the bottom of the downcomers with the most important dimensions.

2.7. Atmospheric multi-stage fluidized bed desorber

To make this technology suitable for sour gas removal from natural gas, the sorbent fed to the adsorber has to be very lean because the natural gas specifications are tight (<3.5 ppm for H_2S). The required maximum lean sorbent loading is then determined by the adsorption isotherm. To ensure that the extent of desorption in the desorber is not limiting, the desorber design was oversized. The multi-stage fluidized bed desorber is operated at atmospheric pressure and consists of seven stages. The inner diameter of the desorber is 200 mm. Per tray two downcomers were installed with an inner diameter of 20 mm. The bed height of each bed in the desorber is 100 mm. Perforated plates were used as gas distributors, except for the lowest stage which uses a sintered plate. Also here horizontal plates with a diameter equal to the outer diameter of the downcomer were installed 16 mm below the bottom of the downcomer to prevent excessive fluidization in the downcomer. N_2 was used as stripping gas with a typical superficial velocity of 0.15 m/s. The wall of the desorber is heated using electrical heat tracing, the target temperature for each tray was 100 °C. K-type thermocouples in thermowells were used to measure the bed temperature 20 mm above the gas distributor at each tray.

2.8. Operation and other details of the pilot plant

During assembly of the pilot plant each tray of the adsorber and desorber and each vessel was filled with an initial amount of sorbent. The pilot plant is started by introducing the N_2 flow to the desorber and enabling the heating of the desorber. Afterwards a small N2 flow (~10 SL/min) was introduced to the adsorber. The adsorber was pressurized to the operating pressure with the back pressure regulator and the N_2 flow was increased to the desired setpoint while tuning the back pressure regulator to compensate for the pressure increase. When the operating pressure of the adsorber was set, the pressurizing sequence of the HP/LP and LP/HP lock were turned on and tuned to match the operating pressures. Now the sorbent flow was started with the rotary valves. The sorbent flow is controlled via the rotary valve below the desorber: this rotary valve always turned slower than

the other rotary valves. The sorbent flow was regulated via a variable-frequency drive and found to be a linear function of the sorbent flow. When the setup was circulating sorbent continuously, the desired inlet concentration could be set, which was measured via a bypass.

In the experimental campaign the superficial velocity in the adsorber was set at $1.25u_{mf}$ for each pressure. This is a low fluidization velocity, but homogenous fluidization of the bed was still observed. The superficial velocity was kept at this value because the operating window is narrow for the given design: increasing the superficial gas velocity resulted in upward sorbent transport in the adsorber (flooding). Consequently, this is an important aspect of future design of (pressurized) MSFBs. Explicitly, the design of the gas distributor, the height of the fluidized bed and the downcomer dimensions are important aspects. The sorbent flux, defined as the sorbent flow per unit of cross-sectional surface area, was varied between 1.02 and 3.06 kg/(m_R^2 s). The inlet concentration ranged from 4800 to 37,300 ppm. The distance between the gas distributor and the top of the downcomer, and thus the bed height, in the adsorber was varied between 70 and 130 mm. The adsorber pressure was varied between 2 and 10 bara. Steady-state operation of the pilot plant was achieved typically after 3 h. On average one experimental run took 6 h, including start-up, reaching steady state and gas sampling.

3. Results and discussion

3.1. Minimum fluidization at elevated pressures

Table 1 shows the minimum fluidization velocities and bed voidages at minimum fluidization of the amine sorbent for various pressures. The minimum fluidization velocities decreases with increasing pressures, which can be explained by increased drag forces due to the increasing gas density [2]. The bed voidage at minimum fluidization ε_{mf}, calculated via Eq. 1, can be considered pressure independent. These two trends are in line with previous findings by Sobreiro and Monteiro who also investigated the pressure behavior of Geldart B particles [16].

$$\Delta P = (1-\varepsilon_{mf})\left(\rho_s-\rho_g\right)gH \tag{1}$$

According to Wen and Yu minimum fluidization conditions can be predicted by [17]:

$$K_1\ \mathrm{Re_{p,mf}}^2 + K_2\ \mathrm{Re_{p,mf}} = \mathrm{Ar} \Leftrightarrow \mathrm{Re_{p,mf}} = \left[\left(\frac{K_2}{2K_1}\right)^2 + \frac{1}{K_1}\cdot \mathrm{Ar}\right]^{1/2} - \frac{K_2}{2K_1} \tag{2}$$

In this equation K_1 and K_2 are constants, $\mathrm{Re_{p,mf}}$ is the particle Reynolds number at minimum fluidization and Ar is the Archimedes number:

$$\mathrm{Re_{p,mf}} = \frac{d_p u_{mf}\rho_g}{\mu} \quad \text{and} \quad \mathrm{Ar} = \frac{d_p^3\rho_g\left(\rho_s-\rho_g\right)g}{\mu^2} \tag{3}$$

The particle size distribution of the amine sorbent has been measured, of which the results are shown in Section 1 of the supplementary information. We choose to use the Sauter mean diameter as input parameter for $\mathrm{Re_{p,mf}}$ and Ar, which is found to be 631 μm (Section 1 of the supplementary information). Fig. 7 shows the developed correlation for $\mathrm{Re_{p,mf}}$ of the used amine sorbent, together with a comparison with some frequently used literature correlations [17,18]. The fitted constants are $K_1 = 27.7$ and $K_2 = 2.02 \cdot 10^3$, which yields the correlation for the minimum fluidization of the used amine sorbent:

$$27.7 \cdot\ \mathrm{Re_{p,mf}}^2 + 2.02 \cdot 10^3 \cdot\ \mathrm{Re_{p,mf}} = \mathrm{Ar} \tag{4}$$

Fig. 7 shows that the existing literature correlation overpredict $\mathrm{Re_{p,mf}}$, and thus the minimum fluidization velocity. The experimental data fit well to the correlation. eq:corrumf is used for calculating intermediate values of the minimum fluidization velocities throughout this work.

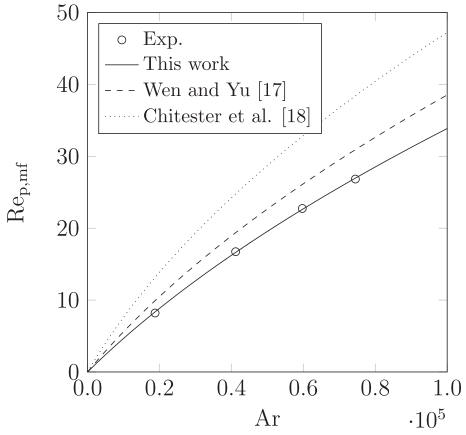

Fig. 7. Correlation for minimum fluidization conditions for different pressures. The solid line represents the fitted correlation of this work.

3.2. Breakthrough experiments in the one stage fluidized bed adsorber

Fig. 8 shows the effect of pressure on the adsorption of CO_2 on the amine sorbent in the one stage fluidized bed adsorber (Fig. 2). The superficial velocity was kept at $u_0 = 1.5u_{mf}$, where u_{mf} was evaluated according to Fig. 7. The pressure trend can clearly be seen: increased pressures lead to faster adsorption rates and, thus, breakthrough is observed earlier. This is a result of multiple effects which happen if the pressure increases. First, the CO_2 partial pressure increases because a fixed inlet mole fraction is used, and so the equilibrium sorbent loading increases. Second, the CO_2 molar flow rate increases. Third, the intrinsic adsorption kinetics will be faster. Fourth, regarding fluidization and

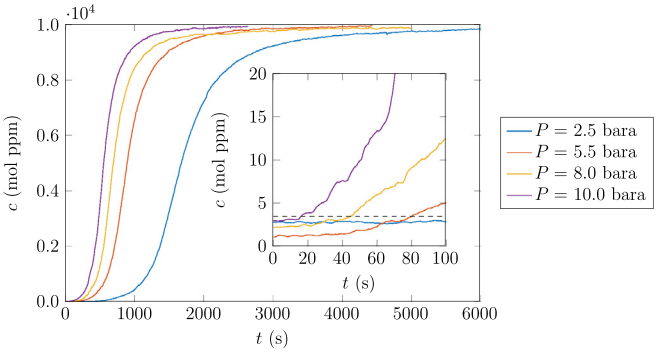

Fig. 8. CO_2 adsorption breakthrough curves in a fluidized with various pressures at $u_0 = 1.5u_{mf}$ and a fixed inlet mole fraction (c_{in} = 10000 mol ppm, fixed bed height = 0.226 m). The inset magnifies the data in the first seconds. The dashed line in the inset indicates the H_2S specification in natural gas.

Table 1
Minimum fluidization velocities and bed voidages at different pressures.

P (bara)	u_{mf} (m/s)	ε_{mf} (m_g^3/m_R^3)
2.5	0.082	0.518
5.5	0.076	0.516
8	0.071	0.516
10	0.067	0.514

hydrodynamics one could state that fluidization at elevated pressures is more homogeneous from which gas-solid contacting benefits [19].

The inset in Fig. 8 shows the measured outlet concentrations in the first seconds of the measurement. It can be seen that the concentration is lower than the H_2S specification of 3.5 ppm for any pressure in the first seconds. Even for $P = 10.0$ bara, the concentration is below 3.5 mol ppm in the first 16 s. Please note the start concentrations of the breakthrough curve: they are already a few mol ppm. Furthermore, these low concentrations are approaching the detection limit of the used analyzer. It is very likely that the CO_2 analyzer overestimates the actual concentration: as shown in previous work the CO_2 analyzer indicated a concentration of 3.9 mol ppm while measuring a calibrated CO_2/N_2 mixture of 2.9 ± 0.1 mol ppm [4]. To conclude, these breakthrough measurements already show that it is likely that the specification of <3.5 mol ppm can be reached, also when circulating the sorbent in the continuous setup, with the condition that the sorbent is lean enough.

3.3. Pressurized MSFB pilot plant

3.3.1. Measurement errors and reproducibility

The reported concentrations and temperatures are averaged over at least 120 s. The 95% confidence intervals for concentration were calculated over this time period and it was found that the 95% confidence intervals were generally smaller than 1% of the measured concentration. Therefore, no error bars are shown in any of the presented concentration profiles. With respect to temperature, K-type thermocouples have an measurement error of ±1.5 °C according to thermocouple standards.

To check the reproducibility of the measurements, one measurement was executed twice with identical operating parameters. The concentration and temperature profile of the two identical measurements are shown in Fig. 9. The agreement between the two measurements is fair. There are slight differences in the concentration profile, which may be caused by the difference in temperature. Although the adsorber wall is cooled with cooling water, the temperature of the surroundings do influence the measurement because the thermostat bath did not have enough power to cool it completely. The resemblance of the two measurements ensures reproducibility.

3.3.2. Pressure drops

The pressure drop across stage $n = 2$ (that is, across the perforated plate and the fluidized bed) is 5.7 mbar at a superficial gas velocity of 0.084 m/s and a bed height of 130 mm. Using the orifice theory as reported in the book of Kunii and Levenspiel [2], the pressure drop across the perforated plate (2.5% open area) is 1.8 mbar. Neglecting other possible pressure losses such as drag, the pressure drop across the fluidized bed is 3.9 mbar. Hereby, the ratio between the pressure drop of the perforated plate and the fluidized bed is 45%, which fulfills the rule of thumb for proper gas distribution in fluidized beds. The pressure drop across the metal sintered plate for stage $n = 1$ was not measured, but will definitely be higher than the pressure drop across the perforated plate. An important thing to note is that the gas will partly flow through the downcomers from stage to stage, but this could not be measured or quantified.

3.3.2.1. Process parameter variations. The gas-based Murphree tray efficiency is used to describe the extent to which equilibrium is reached:

$$E^{G}_{\text{tray},n} = \frac{c_{n-1} - c_n}{c_{n-1} - c^*_n(q_n, T_n)} \tag{5}$$

In this equation n is the stage number (the bottom stage corresponds to $n = 1$ as shown in Fig. 5), c^*_n is the gas concentration in equilibrium with the outgoing sorbent loading q_n and the stage temperature T_n. This definition implicitly assumes that each tray is ideally mixed which means that the outlet gas concentration and outlet sorbent loading are equal to respectively the gas concentration and sorbent loading at each tray. To describe the adsorption equilibrium the CO_2 adsorption isotherm on the amine sorbent as fitted by Bos et al. is used [12], because this adsorption isotherm corresponds to the applied CO_2 partial pressures in this work (0 − 0.37 bar). The sorbent loading q_n is calculated via a mass balance over the adsorber. For more information about various definitions of tray efficiencies, we refer to earlier published work [4].

To calculate the sorbent loading q_n, the sorbent loading of the sorbent entering the adsorber has to be known. The assumption is made that the inlet sorbent loading of the adsorber can be neglected, which is supported by three arguments. First, the sorbent residence time in the desorber is 24 min for the highest solid flux and 71 min for the lowest solid flux, which is long enough to desorb the CO_2 from the amine sorbent [3]. Second, the sorbent loading leaving the desorber can be estimated by measuring the concentration of the bottom stage of the desorber. The CO_2 desorption rate of the used amine sorbent is limited by heat transfer: the intrinsic desorption rate and mass transfer processes are rather fast at elevated temperatures, which means that the gas concentration and sorbent loading are in equilibrium with each other [20]. A gas connection was made at the top of the bottom stage of the desorber to sample the gas at that stage and measure the CO_2 concentration. The latter was done for a typical measurement ($P = 10$ bara, $c_{in} = 10000$ mol ppm, $u_0 = 0.084$ m/s, $S = 2.05$ kg/(m^2_R s), $H = 130$ mm) and the measured concentration at the bottom stage was 54 mol

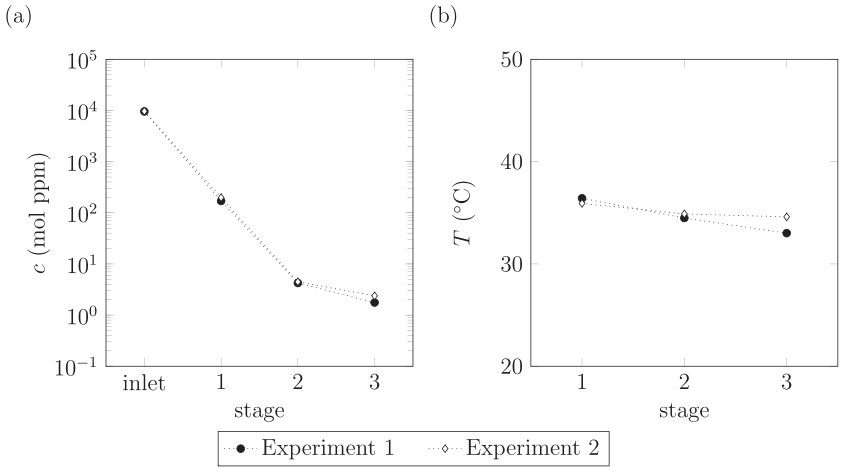

Fig. 9. Concentration and temperature profiles of two identical measurements. ($P = 10$ bara, $c_{in} = 10000$ mol ppm, $u_0 = 0.084$ m/s, $S = 2.05$ kg/(m^2_R s), $H = 130$ mm).

ppm at a temperature of 108 °C. According to the adsorption isotherm the sorbent loading in equilibrium with this CO_2 partial pressure and temperature is $1.4 \cdot 10^{-3}$ mol/kg. Using a similar approach as previous work, it is concluded that the error in the reported tray efficiencies is always smaller than 0.001 units and that the reported tray efficiencies are on the conservative side [4]. Third, when leaving the desorber the sorbent remains in a N_2 atmosphere for a while (riser, cyclone, buffer vessel, HP/LP lock and again a buffer vessel) in which CO_2 still can desorb. To conclude, it is fair to assume that the sorbent loading of the sorbent entering the adsorber can be neglected.

Fig. 10 shows the effect of varying solid flux on the measured concentration and tray efficiency. The column profiles including temperature can be found in Section 2 of the supplementary information. Increasing the solid flux results in lower concentrations, because more sorbent is available to adsorb the same amount of CO_2. One can see that the concentration lowers from 20,000 mol ppm to less than 10 mol ppm for every solid flux, while the gas residence time of the gas is only 0.5 s. This fast process is only possible if the contacting between the sorbent and the gas is good, if adsorption kinetics are fast and if intraparticle mass transfer is fast enough to keep up with the adsorption rate. The H2S specification c_{spec} of 3.5 mol ppm is not reached within three stages but the measured concentrations do approach it and a further fourth stage is expected to be sufficient. With respect to tray efficiencies, at stage the bottom $n = 1$ and $n = 2$ the tray efficiencies are high, they are larger than 0.85 and often larger than 0.90, which means that equilibrium is almost reached. A slight trend in the tray efficiency can be observed: higher solid fluxes lead to larger tray efficiencies, certainly at stage 1 in Fig. 10b. A likely explanation is that higher solid fluxes lead to a lower fractional coverage of the adsorption sites and, hence, more free sites are available for CO_2 adsorption. The tray efficiencies at the top stage $n = 3$ are significantly lower; however, this is a consequence of the design of the top stage as will be discussed later.

The effect of inlet concentration is shown in Fig. 11. This figure proves that the H2S specification c_{spec} of 3.5 mol ppm can indeed be reached: the measurements at $c_{in} = 10600$ mol ppm and $c_{in} = 4800$ mol ppm have outlet concentrations (much) lower than 3.5 mol ppm. Furthermore, the measurement at $c_{in} = 37300$ mol ppm still has an outlet concentration as low as 5.6 mol ppm. Therefore, this pressurized MSFB technology is able to remove gas impurities over a wide range of inlet concentrations: from bulk (>2%) to deep removal (<0.1%). Also here the tray efficiencies remain larger than 90%. Again, the tray efficiencies at stage 3 show differences related to the design of the top stage.

Fig. 12 shows the effect of pressure on the measured concentrations and tray efficiencies when the inlet composition is set at a fixed mole fraction. The superficial velocity was kept at $1.25u_{mf}$, where u_{mf} was evaluated for each pressure using Fig. 7. Although pressure has a large impact on phenomena such as fluidized bed hydrodynamics, equilibrium loading, mass transfer and adsorption kinetics, only a small trend is observed. Lower pressures lead to lower stage concentrations and larger tray efficiencies but differences are rather small, certainly when considering the logarithmic scale of Fig. 12a. At lower pressures less CO_2 has to be removed to arrive at a low CO_2 mole fraction, which may explain this trend. The concentration profiles behave like if the process is first order in the CO_2 partial pressure, that is, c_n/c_{n-1} is constant. Attributing the observed trend to one of the mentioned phenomena deserves and requires more research. In any case, the tray efficiencies at stage $n = 1$ and $n = 2$ remain larger than 95%.

The measurement series in fig:Pvar may be biased because the CO_2 molar flow (mol_{CO_2}/s) also changes with pressure if the mole fraction is kept constant. Therefore, a measurement series was conducted where the adsorber pressure was varied but the CO_2 molar flow was kept constant. In this way the pressure only has an influence on the fluidized bed hydrodynamics. The results are shown in Fig. 13. For interpretation, the concentrations have been normalized with the inlet concentration in Fig. 14, which shows that c_n/c_{in} is more or less constant, which suggests that the process is first order in the gas concentration. Furthermore, from this figure one can conclude that changes in hydrodynamics due to pressure do not have a significant effect on the CO_2 removal.

Multi-stage fluidized beds for adsorption typically employ shallow fluidized beds. Therefore, fig:Hvar investigates the effect of the bed height H on the concentrations and tray efficiencies. From this figure it can be concluded that the major part of the CO_2 adsorption process happens just above the gas distributor. As an example, the bed height is increased from $H = 70$ mm to $H = 130$ mm, but the concentration at stage $n = 2$ only decreases from 13 mol ppm to 4 mol ppm and there is almost no effect on the tray efficiency. Just above the gas distributor the contact between gas and sorbent is rather good because of small bubbles and bubble throughflow, which supports this statement [2,21]. Therefore, it is recommended to invest in more trays, so more equilibrium stages can be obtained, rather than investing in deeper fluidized beds.

As discussed before, the tray efficiencies at the top stage $n = 3$ show a different trend compared to stages $n = 1$ and $n = 2$. We hypothesize that the sorbent bypasses the top stage $n = 3$ by falling directly from the rotary valve in the downcomer from the top stage $n = 3$ to stage $n = 2$ (Fig. 5). This reduces the effective amount of lean sorbent entering the

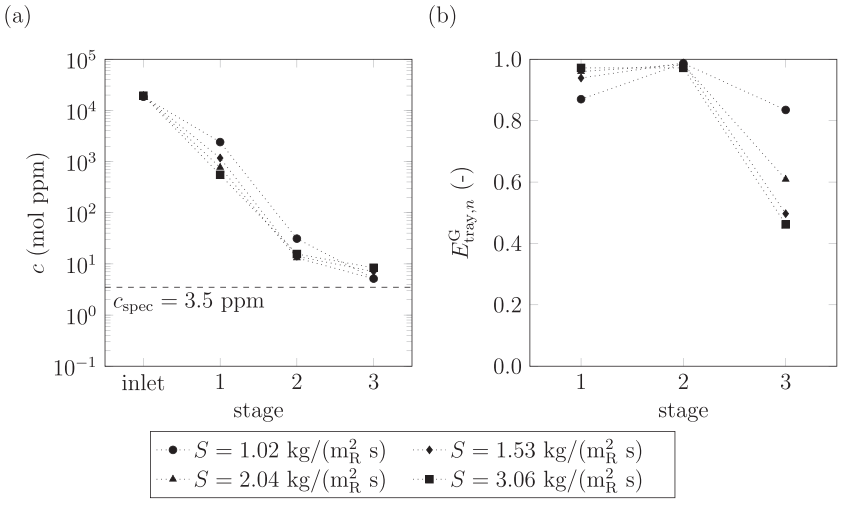

Fig. 10. Column profiles for varying solid flux: (a) concentration and (b) tray efficiency. ($P = 10$ bara, $c_{in} = 20000$ mol ppm, $u_0 = 0.084$ m/s, $H = 130$ mm).

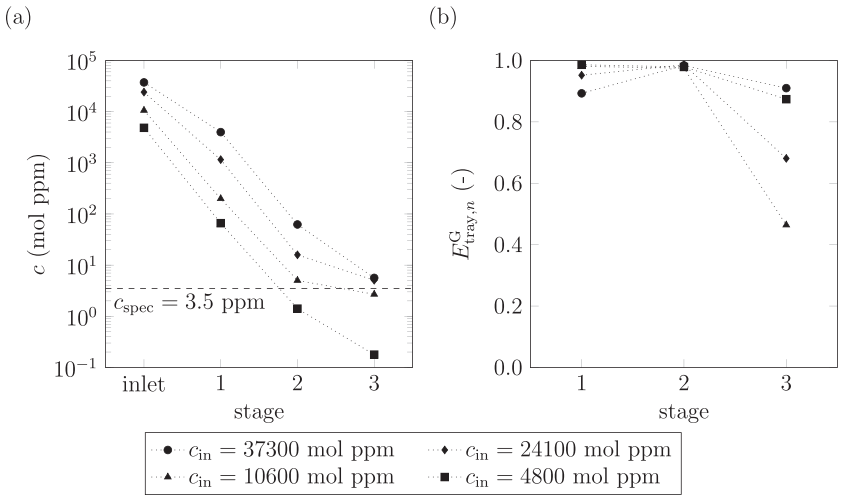

Fig. 11. Column profiles for varying inlet concentrations: (a) concentration and (b) tray efficiency. ($P = 10$ bara, $S = 2.04$ kg/(m^2_R s), $u_0 = 0.084$ m/s, $H = 130$ mm).

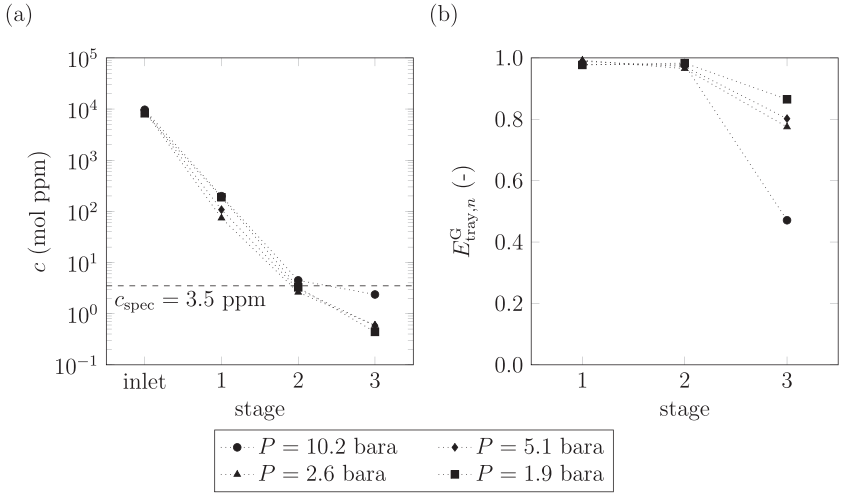

Fig. 12. Column profiles for varying adsorber pressures: (a) concentration and (b) tray efficiency. ($c_{in} = 10000$ mol ppm, $S = 2.04$ kg/(m^2_R s), $u_0 = 1.25u_{mf}$ for each pressure, $H = 130$ mm).

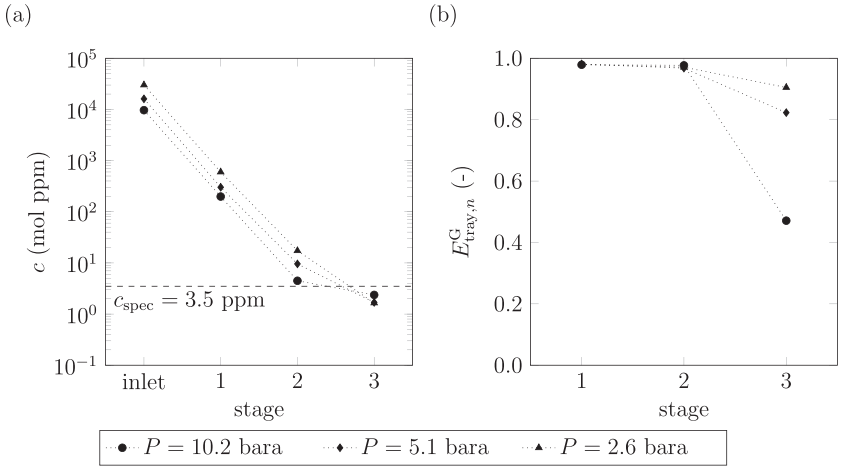

Fig. 13. Column profiles for varying adsorber pressures where the CO_2 partial pressure is kept constant: (a) concentration and (b) tray efficiency. ($S = 2.04$ kg/(m^2_R s), $u_0 = 1.25u_{mf}$, $H = 130$ mm, $P_{CO2} = 0.08$ bar).

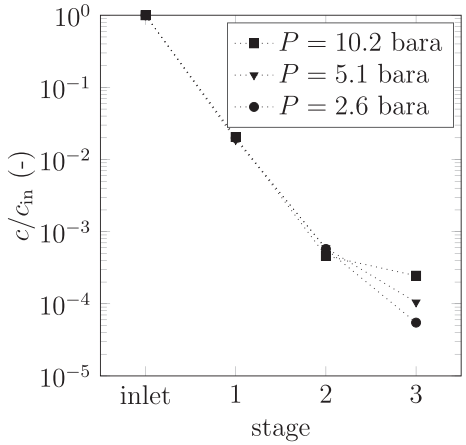

Fig. 14. Normalized concentration profile for varying adsorber pressures where the CO_2 partial pressure is kept constant. ($S = 2.04$ kg/(m_R^2 s), $u_0 = 1.25u_{mf}$, $H = 130$ mm, $P_{CO2} = 0.08$ bar).

third stage. To confirm this hypothesis, a horizontal plate with a diameter equal to the downcomer diameter was installed above the top of the downcomer at the top stage $n = 3$. This horizontal plate prevents bypassing of the lean sorbent, so all lean sorbent enters the bed. The results of this experiment are shown in Fig. 16. This figure clearly shows that the concentration indeed lowers if bypassing of sorbent is prevented. In addition, the tray efficiency also significantly improves. Furthermore, in Figs. 10–15 there are multiple data points where the concentration is smaller than 10 mol ppm while having a tray efficiency larger than 0.9 at stage $n = 2$. To conclude, the tray efficiencies remain high over a wide concentration range as long as sorbent bypassing is prevented in the design of the MSFB.

3.4. Investigating mass transfer processes

From the experiments it is concluded that the mass transfer processes have to be fast: in just a few seconds the gas concentration is reduced from 37,300 mol ppm to 6 mol ppm for example (Fig. 11). However, the question remains to what extent various mass transfer processes do influence or limit the adsorption rate of CO_2. This is investigated using a numerical particle including intrinsic adsorption kinetics [12], intraparticle mass transfer and external mass transfer from gas to particle. The modeling equations and input parameters can be found in Section 3 of the supplementary information. The goal of this simulation is to investigate the mass transfer processes in a semi-qualitative manner: it does involve modeling of a single particle, but with typical - and not necessarily exact - values of parameters and properties. The CO_2 adsorption rate from the particle model is compared to the experimental CO_2 adsorption rate and they have the same order of magnitude.

In the simulation a fully desorbed single particle is followed when it enters the top stage $n = 3$ of the adsorber, through stage $n = 2$ and eventually to the bottom stage $n = 1$. It is assumed that the gas phase of each stage is ideally mixed, which implies that the particle is confronted with three different bulk concentrations (three stages) for a time equal to the residence time of the particle in a stage. As reference measurement the experiment with $c_{in} = 37300$ mol ppm from Fig. 11 is taken because of its excessive concentration difference between inlet and outlet. In this measurement the residence time of a particle in each stage is 27 s. All stages are assumed to have a homogeneous bed temperature of 35 °C. Intraparticle heat transfer limitations are neglected. The influence of external mass transfer, intraparticle mass transfer and intrinsic adsorption kinetics is then investigated by varying respectively the external mass transfer coefficient, the effective pore diffusion coefficient and the intrinsic adsorption rate constant. From preliminary simulations it was concluded that in terms of qualitative behavior stage $n = 2$ and $n = 1$ behave very similar. Therefore, only the results for the bottom stage $n = 1$ ($c_1 = 3982$ mol ppm) and the top $n = 3$ ($c_3 = 5.6$ mol ppm) are shown.

Fig. 17 shows the effect of external mass transfer on the adsorption rate. The Sherwood number of a particle in the pressurized MSFB adsorber was calculated based on the correlation of Gunn [22]. Besides this reference case (where $Sh = k_g d_p / D_{AB} = 12.6$, [22]), two limit situations are shown: $Sh = 2$ which represents the limit of a particle in a stagnant medium and $Sh = \infty$ which represents no external mass transfer resistance. At the top stage $n = 3$ of Fig. 17a the CO_2 adsorption rate does not vary that much with time (<17%), because the increase in sorbent loading is such low that it does not effect the adsorption rate. The theoretical consequences of this observation will be discussed later in more detail. In addition, with respect to the top stage $n = 3$ (Fig. 17a) it can be concluded that the effect of external mass transfer is minor: when eliminating any external mass transfer resistance the adsorption rate increases only by ~10 %. At the bottom stage $n = 1$ (Fig. 17b) the adsorption rate decreases over time due to decreasing adsorption kinetics because of increasing CO_2 sorbent loading. Also here the effect of external mass transfer is almost negligible.

Fig. 18 shows the effect of the effective pore diffusion coefficient for three cases: the reference case with the actual (estimated) value of the effective pore diffusion coefficient $D_{p,ref} = 1.15 \cdot 10^{-7}$ m^2/s, a case where the effective pore diffusion coefficient is increased tenfold and a case where it is decreased tenfold. For the top stage $n = 3$

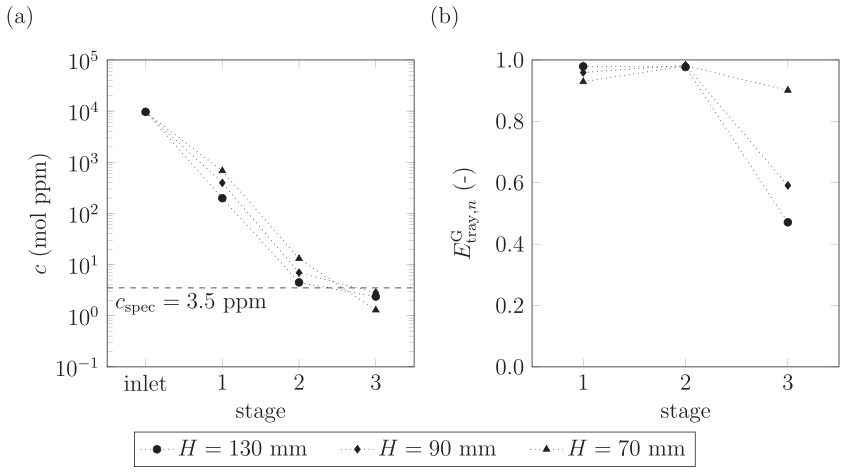

Fig. 15. Column profiles for varying bed heights: (a) concentration and (b) tray efficiency. ($c_{in} = 10,000$ mol ppm, $S = 2.04$ kg/(m_R^2 s), $u_0 = 0.084$ m/s, $P = 10$ bara).

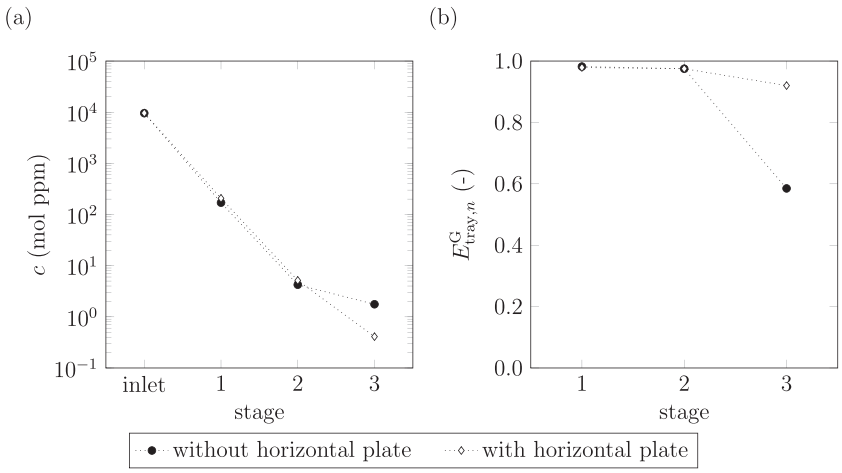

Fig. 16. The effect of a horizontal plate at the top of the downcomer at the top stage $n = 3$: (a) concentration and (b) tray efficiency. ($P = 10$ bara, $c_{in} = 10,000$ mol ppm, $u_0 = 0.084$ m/s, $S = 2.05$ kg/(m^2_R s), $H = 130$ mm).

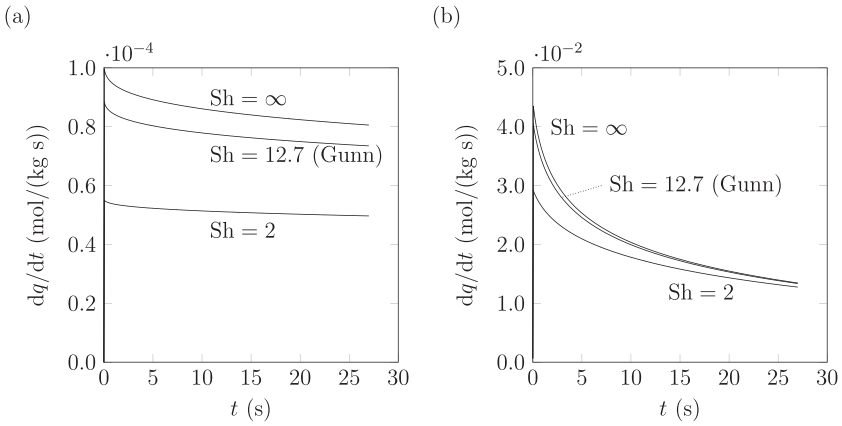

Fig. 17. The effect of external mass transfer on the adsorption rate: (a) the top stage $n = 3$ and (b) the bottom stage $n = 1$. Three cases are shown: no external mass transfer resistance (Sh $= \infty$), external mass transfer for a typical fluidized bed (Sh $= 12.6$, [22]) and external mass transfer in a stagnant medium (Sh $= 2$).

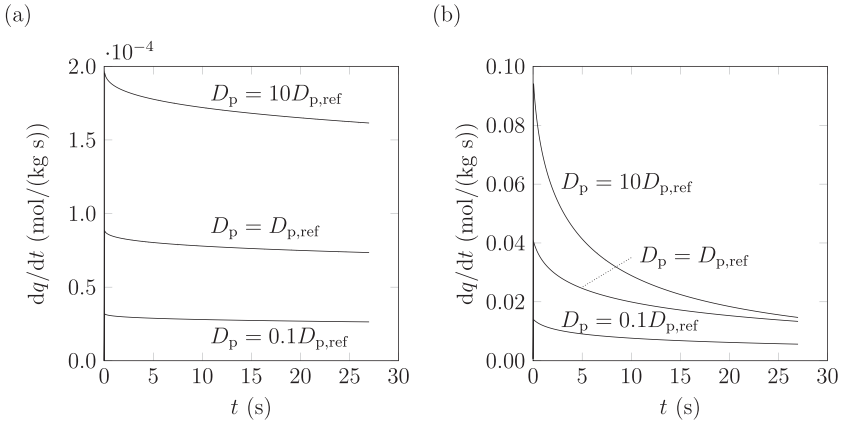

Fig. 18. The effect of intraparticle diffusion on the adsorption rate: (a) the top stage $n = 3$ and (b) the bottom stage $n = 1$. Three cases are shown: the reference case with the actual effective pore diffusion coefficient $D_{p,\,ref}$, a case where $D_{p,\,ref}$ is increased with a factor 10 and a case where $D_{p,\,ref}$ is decreased with a factor 10.

(Fig. 18a) the effect of the effective pore diffusion coefficient is strong. Also here the effect of time and, thus, sorbent loading on the CO_2 adsorption rate is minor. For the bottom stage $n = 1$ (Fig. 18b) the effect of the effective pore diffusion coefficient reduces over time because the adsorption rate decreases and, hence, intraparticle diffusion limitations decrease.

Fig. 19 shows the effect of the intrinsic adsorption rate constant k_T on the adsorption rate for three cases analogous to the approach of the

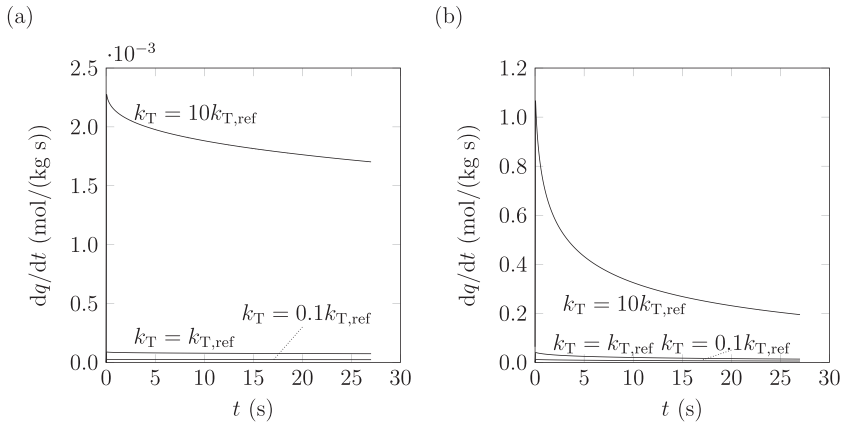

Fig. 19. The effect of adsorption kinetics on the adsorption rate: (a) the top stage $n = 3$ and (b) the bottom stage $n = 1$. Three cases are shown: the reference case with the actual intrinsic adsorption rate constant $k_{T,\,ref}$, a case where $k_{T,\,ref}$ is increased with a factor 10 and a case where $k_{T,\,ref}$ is decreased with a factor 10.

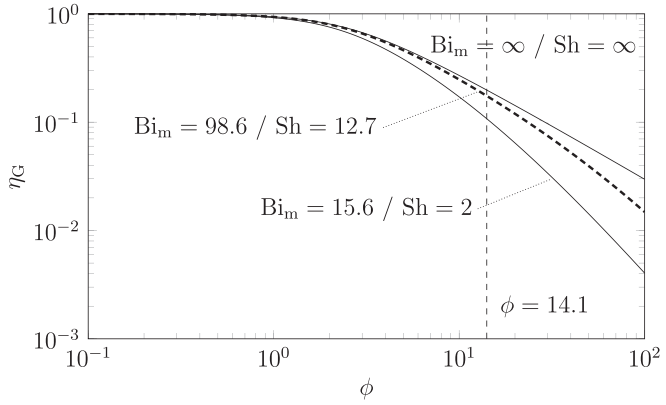

Fig. 20. The analytical solution for the global effectiveness factor including intraparticle diffusion and external mass transfer [23]. The vertical dashed line represents the Thiele modulus ($\phi = 14.1$) of the particle and the thick dashed line represents the modified Sherwood number of the particle ($Bi_m = 98.6$).

effective pore diffusion coefficient. The reference intrinsic adsorption rate constant is $k_{T,\,ref} = 9.27$ mol/(kg bar s). Again at the top stage $n = 3$ (Fig. 19a) the adsorption rate does not vary much with time (<12%) and, thus, sorbent loading. For the bottom stage $n = 1$ (Fig. 19b) the decline in the adsorption rate due to the increasing sorbent loading can be observed.

As observed, the CO_2 adsorption rate is independent of time, and so sorbent loading, at the top stage $n = 3$. Besides, the sorbent loading at the top stage $n = 3$ is approximately zero because not much CO_2 can adsorb. These two arguments lead to the conclusion that the intrinsic adsorption rate can effectively be approached by a first order reaction in the gas concentration. An analytical solution for the global effectiveness factor, which includes the intraparticle diffusion and external mass transfer resistances, can be used for interpretation [23]. Fig. 20 shows the analytical solution for the global effectiveness factor for a spherical particle η_G as function of the Thiele modulus $\phi = L \cdot \sqrt{\rho_s k_T RT / D_p}$ and the Biot number for mass transfer $Bi_m = k_g L / D_p$. Please note that (a) L represents the radius of the particle - not its diameter - and (b) that the Biot number for mass transfer uses the effective pore diffusion coefficient - and not the molecular diffusivity. The Thiele modulus of the system is $\phi = 14.1$ and the Biot number for mass transfer is $Bi_m = 98.6$. Two conclusions can be drawn. First, fig:global_eff shows that the adsorption rate of CO_2 is mainly limited by intraparticle mass transfer. Even for infinitively fast external mass transfer ($Sh' = \infty$), the global effectiveness factor is $\eta_G = 0.20$. Second, the global effectiveness including a typical fluidized bed external mass transfer resistance ($Bi_m = 98.6$), is $\eta_G = 0.17$ which shows that the combination of intraparticle and external mass transfer poses serious limitations on the CO_2 adsorption rate.

The conclusions above are valid for low sorbent loadings - that is, the top stage $n = 3$ - but may be less valid for the bottom stage $n = 1$ where the sorbent loadings are higher. In Figs. 17b, 18b and 19b the effect of increasing sorbent loading on the adsorption kinetics can clearly be observed, because the adsorption rate does decrease over time. However, the CO_2 adsorption rate does not decrease with orders of magnitude within the residence time of the particle in a stage of the adsorber. Therefore, it seems reasonable to state that also here the CO_2 adsorption rate is limited by intraparticle mass transfer. To conclude, for the presented measurements intraparticle mass transfer does control the CO_2 adsorption rate, both at low ($c < 10$ mol ppm) and high concentration ($c > 10,000$ mol ppm). The latter allows opportunities to engineer a sorbent particle that does not suffer from intraparticle diffusion limitations to the same extent, for example by using smaller particles.

4. Conclusion

This research focuses on a pilot plant scale experimental setup where CO_2 is removed from a gaseous stream using a pressurized MSFB in a continuous adsorption process. The adsorption was performed at elevated pressure, while the desorption was performed at atmospheric pressure. The operation at two pressure levels requires that the sorbent is pressurized before entering the adsorber and is depressurized before entering the desorber. This unit operation is executed in a so-called LP/HP or HP/LP lock. The proposed pressurized MSFB technology could reduce the size for PSA processes, because the sorbent is used more effectively and heat transfer is faster compared to fixed bed adsorption processes.

The built setup shows that continuous PSA in a pressurized MSFB is technically possible and it has been demonstrated for the first time. The removal efficiency are high: a removal from 37,000 mol ppm CO_2 down to <10 mol ppm CO_2 has been measured while the residence time of the gas was only a few seconds. The latter shows that the gas concentration can be reduced over decades in concentration and that this technology may be used for sour gas removal to natural gas specifications. Tray efficiencies were often >0.85, implying that equilibrium is approached at each stage. As long as sorbent bypassing is prevented during the design of the stage, it is expected that tray efficiencies will be high. Hydrodynamic changes due to differences in pressure do not effect the CO_2 removal.

Mass transfer on a particle level was investigated with a numerical model, from which it was concluded that intraparticle mass transfer limitations dominate the CO_2 adsorption rate. Even faster adsorption

of CO_2 can be realized by engineering a future amine sorbent in a way that intraparticle diffusion limitations are eliminated. Already at this development level this MSFB technology shows an excellent CO_2 adsorption rate providing potentially compact equipment in comparison with PSA processes.

Acknowledgments

This research was carried out in the context of the Compact Advanced Sour gas Processing (CASPer) project, coordinated by the Institute for Sustainable Process Technology (ISPT) and co-financed by the Ministry of Economic Affairs of the Netherlands (RVO.nl project number TEEI115008). The experimental setup could not have been built and operated without the technical support of Johan F.H. Agterhorst and Karst van Bree (Sustainable Process Technology group, University of Twente).

Appendix A. Supplementary data

Supplementary data to this article can be found online at https://doi.org/10.1016/j.powtec.2020.03.013.

References

[1] J.D. Seader, E.J. Henley, D.K. Roper, Separation Process Principles, John Wiley & Sons, Inc, 2011.
[2] D. Kunii, O. Levenspiel, Fluidization Engineering, 2nd edition Butterworth-Heinemann, 1991.
[3] R. Veneman, T. Hilbers, D.W.F. Brilman, S.R.A. Kersten, CO_2 capture in a continuous gas-solid trickle flow reactor, Chem. Eng. J. 289 (2016) 191–202, https://doi.org/10.1016/j.cej.2015.12.066.
[4] R.T. Driessen, M.J. Bos, D.W.F. Brilman, A multistage fluidized bed for the deep removal of sour gases: proof of concept and tray efficiencies, Ind. Eng. Chem. Res. 57 (11) (2018) 3866–3875, https://doi.org/10.1021/acs.iecr.7b04891.
[5] D. Das, D.P. Samal, B.C. Meikap, Removal of CO_2 in a multistage fluidized bed reactor by diethanol amine impregnated activated carbon, J. Environ. Sci. Health A 51 (9) (2016) 769–775, https://doi.org/10.1080/10934529.2016.1170462.
[6] S. Roy, C.R. Mohanty, B.C. Meikap, Multistage fluidized bed reactor performance characterization for adsorption of carbon dioxide, Ind. Eng. Chem. Res. 48 (23) (2009) 10718–10727, https://doi.org/10.1021/ie901133r.
[7] G. SchÃny, E. Zehetner, J. Fuchs, T. PrÃll, G. Sprachmann, H. Hofbauer, Design of a bench scale unit for continuous CO_2 capture via temperature swing adsorption - fluid-dynamic feasibility study, Chem. Eng. Res. Des. 106 (2016) 155–167, https://doi.org/10.1016/j.cherd.2015.12.018.
[8] G. Schöny, F. Dietrich, J. Fuchs, T. Pröll, H. Hofbauer, A multi-stage fluidized bed system for continuous CO_2 capture by means of temperature swing adsorption – first results from bench scale experiments, Powder Technol. 316 (2017) 519–527, https://doi.org/10.1016/j.powtec.2016.11.066.
[9] F. Dietrich, G. Schöny, J. Fuchs, H. Hofbauer, Experimental study of the adsorber performance in a multi-stage fluidized bed system for continuous CO_2 capture by means of temperature swing adsorption, Fuel Process. Technol. 173 (2018) 103–111, https://doi.org/10.1016/J.FUPROC.2018.01.013.
[10] G.G. Nasr, N.E. Connor, Natural Gas Engineering and Safety Challenges, Springer International Publishing, 2014https://doi.org/10.1007/978-3-319-08948-5_1.
[11] Q. Yu, J. Delgado, R. Veneman, D.W.F. Brilman, Stability of a benzyl amine based CO_2 capture adsorbent in view of regeneration strategies, Ind. Eng. Chem. Res. 56 (12) (2017) 3259–3269, https://doi.org/10.1021/acs.iecr.6b04645.
[12] M.J. Bos, T. Kreuger, S.R.A. Kersten, D.W.F. Brilman, Study on transport phenomena and intrinsic kinetics for CO_2 adsorption in solid amine sorbent, Chem. Eng. J. (2019) https://doi.org/10.1016/j.cej.2018.11.072.
[13] W.R. Alesi, J.R. Kitchin, Evaluation of a primary amine-functionalized ion-exchange resin for CO_2 capture, Ind. Eng. Chem. Res. 51 (19) (2012) 6907–6915, https://doi.org/10.1021/ie300452c.
[14] S. Sutanto, J.W. Dijkstra, J.A.Z. Pieterse, J. Boon, P. Hauwert, D.W.F. Brilman, CO_2 removal from biogas with supported amine sorbents: first technical evaluation based on experimental data, Sep. Purif. Technol. 184 (2017) 12–25, https://doi.org/10.1016/j.seppur.2017.04.030.
[15] E. Sonnleitner, G. Schöny, H. Hofbauer, Assessment of zeolite 13X and Lewatit VP OC 1065 for application in a continuous temperature swing adsorption process for biogas upgrading, Biomass Convers. Biorefin. (2017) 1–17, https://doi.org/10.1007/s13399-017-0293-3.
[16] L.E.L. Sobreiro, J.L.F. Monteiro, The effect of pressure on fluidized bed behaviour, Powder Technol. 33 (1) (1982) 95–100, https://doi.org/10.1016/0032-5910(82)85043-2.
[17] C.Y. Wen, Y.H. Yu, A generalized method for predicting the minimum fluidization velocity, AIChE J. 12 (3) (1966) 610–612, https://doi.org/10.1002/aic.690120343.
[18] D.C. Chitester, R.M. Kornosky, L.-S. Fan, J.P. Danko, Characteristics of fluidization at high pressure, Chem. Eng. Sci. 39 (2) (1984) 253–261, https://doi.org/10.1016/0009-2509(84)80025-1.
[19] J.G. Yates, Effects of temperature and pressure on gas-solid fluidization, Chem. Eng. Sci. 51 (2) (1996) 167–205, https://doi.org/10.1016/0009-2509(95)00212-X.
[20] M.J. Bos, V. Kroeze, S. Sutanto, D.W.F. Brilman, Evaluating regeneration options of solid amine sorbent for CO_2 removal, Ind. Eng. Chem. Res. 57 (32) (2018) 11141–11153, https://doi.org/10.1021/acs.iecr.8b00768.
[21] L. Tan, I. Roghair, M. van Sint Annaland, Discrete particle simulations of bubble-to-emulsion phase mass transfer in single-bubble fluidized beds, Particuology 33 (2017) 80–90, https://doi.org/10.1016/j.partic.2016.09.008.
[22] D.J. Gunn, Transfer of heat or mass to particles in fixed and fluidised beds, Int. J. Heat Mass Transf. 21 (4) (1978) 467–476, https://doi.org/10.1016/0017-9310(78)90080-7.
[23] D. Murzin, T. Salmi, Catalytic Kinetics, Elsevier, 2005https://doi.org/10.1016/B978-044451605-3/50009-5.

Nomenclature

Symbol: Description (Unit)

Ar: Arrhenius number (–)
Bi_m: Biot number for mass transfer (–)
c: Mole fraction (mol_{CO_2}/mol_g)
D: Diffusion coefficient (m^2/s)
d: Diameter (M)
$E^G_{tray,n}$: Gas-based Murphree tray efficiency (–)
H: Bed height (m_R)
g: Acceleration constant (m/s^2)
$K_{1,2}$: Fitting constants for u_{mf} correlation (–)
k_g: Mass transfer coefficient (m/s)
k_1: Adsorption rate constant ($mol_{CO_2}/(kg_s$ bar s))
L: Particle radius (m_p)
n: Stage number (–)
P: Pressure (Bara)
q: Sorbent loading (mol_{CO_2}/kg_s)
R: Ideal gas constant (J/(mol K))
Re: Reynolds number (–)
S: Solid flux ($kg_s/(m^2_R$ s))
Sh: Sherwood number (–)
T: Temperature
t: Time (S)
u: Superficial gas velocity ($m^3/(m^2_R$ s))
ε: Voidage (m^3_g/m^3_R)
η: Effectiveness factor (–)
μ: Viscosity (Pa s)
ρ: Density (kg/m^3)
ϕ: Thiele modulus (–)

Subscripts/superscripts

AB: Binary
G: Global
g: Gas
mf: Minimum fluidization
p: Particle
ref: Reference
$*$: At equilibrium